CrystEngComm

Accepted Manuscript

Cite this: DOI: 10.1039/c0xx00000x

www.rsc.org/xxxxxx

ARTICLE TYPE

Shape-controlled synthesis of K_2SiF_6:Mn^{4+} nanorods phosphor and luminescent properties

Xiaoqing Li,[#a] Xiangming Su,[#a] Pin Liu,[#a] Jie Liu,[*a] Zhiling Yao,[a] Jiajun Chen,[a] Hui Yao,[a] Xibin Yu,[*a] Ming Zhan[*b]

Received (in XXX, XXX) Xth XXXXXXXXX 20XX, Accepted Xth XXXXXXXXX 20XX
DOI: 10.1039/b000000x

A series of efficient red phosphor K_2SiF_6:Mn^{4+} nanoparticles with uniform morphology and dispersity were successfully prepared through a fast liquid-solid-solution route at room temperature. Potassium oleate and SiO_2 spheres/$KMnO_4$ molar ratio play important role in the formation of nanorods structures. When KOH/oleic acid quality ratio is about 2.5:1 and SiO_2 spheres/$KMnO_4$ molar ratio is about 1:10, the length of nanorods is 1~2 μm and the width is 300~700 nm. Under UV and blue excitation, K_2SiF_6:Mn^{4+} samples show strong red emission, corresponding to the characteristic lines of Mn^{4+}.

1. Introduction

Mn^{4+} doped materials have been extensively studied for lighting, holography, laser, and dosimetry. There is a long list of Mn^{4+} activated red-emitting phosphors, including $SrTiO_3$, Al_2O_3, $YAlO_3$, $Gd_3Ga_5O_{12}$, $CaZrO_3$, $Y_2Sn_2O_7$, MgO.[1] The Mn^{4+} emission wavelengths of these phosphors have broad absorption band in 380~490 nm and sharp emission peaks at 610~760 nm and the emission spectrum show a sharp line corresponding to the spin- and parity-forbidden $^2E_g \rightarrow {}^4A_{2g}$ transition in octahedral sites, are all longer than that of Y_2O_3:Eu^{3+}(611 nm). The main drawbacks of these phosphors are being synthesized by firing host that is costly. Very recently, A series of Mn^{4+} ions doped hexagonal complex alkaline metal fluorides M_2NF_6(M=K, Na, Cs, N=Si, Ge, Zr, Ti, Sn) have been reported to solve this problem. In the previous reports, M_2NF_6: Mn^{4+} has been easily and rapidly prepared by only chemical etching in HF/H_2O solution with the addition of an oxidizing agent at room conditions and presents a strong and broad absorption band in blue region[2, 3].

Nanotechnology has show great promise in many applications, as they usually exhibit electronic, optical, magnetic, and catalytic properties which are distinct as compared to their corresponding bulk materials, but it is well known luminescence efficiency of nanocrystals is drastically lowered[4]. It is predictable that advances in the synthesis of M_2NF_6 nanostructures can drive even more opportunities in this promising field. However, it still remains a tremendous challenge to controllably synthesize M_2NF_6 nanostructures in a facile approach owing to the faster reaction rate. To date, some soft-chemical methods have been used for M_2NF_6 nanostructures with controlled phase, morphology and chemical composition. Pan's group has synthesized $BaSiF_6$:Mn^{4+} nanorods by hydrothermal method[5]. However, the hydrothermal method typically requires high temperature, high pressure and long times. But reports on synthesis of K_2SiF_6:Mn^{4+} nanoparticles are little. Hence, from safety and energy-saving standpoints, the development of a facile room-temperature (RT) solution-phase method to fabricate pure-phase fluoride-based nanoparticles is still eagerly demanded[6].

In this paper, we are in position of using an efficient one-step method at room temperature to solve these problems with taking advantage of all this previous knowledge. The K_2SiF_6:Mn^{4+} nanoparticles that we obtained have perfect uniformity and dispersity, luminescent properties compared to their corresponding bulk materials. Then, we systematically investigated the effect of the reaction parameters (e.g., KOH/oleic acid quality ratio, surfactants, SiO_2 spheres/$KMnO_4$ molar ratio and reaction time) on the shape and luminescent properties. By means of adjusting the synthetic parameters, K_2SiF_6:Mn^{4+} nanoparticles with different sizes, length and width have been obtained.

2. Experimental

2.1. Materials and synthesis

All the chemicals were of analytical grade and used as received without further purification. The raw materials were KOH, oleic acid, ethanol, HF (wt.40%), deionized water, $KMnO_4$, TEOS and ammonium hydroxide.

In our experiments, SiO_2 particles, have a diameter in the range of 100~500 nm and good dispersion, as silicon source, were prepared using TEOS and ammonium hydroxide by the Stober method according to the previous reports[7-9]. In a typical process, KOH (1.2 g) was dissolved into the mixture of deionized water (8 mL), oleic acid (20 mL) and ethanol (8 mL) under magnetic stirring to form homogeneous solution A. Meanwhile, 11 mL HF (wt.40%) solution, 4 mL deionized water and 0.45 g $KMnO_4$ were maxed to form solution B. After that, solution B was added into solution A under magnetic stirring to form solution C. At last, SiO_2 spheres were added into solution C, whilst vigorously

stirring 30 min in room ambient. The molecular ratio of SiO_2 spheres and $KMnO_4$ was 1:10. In order to control the morphologies of K_2SiF_6:Mn^{4+} micro-particles, KOH/oleic acid mass ratio and SiO_2 sphere/$KMnO_4$ molecular ratio were varied. After reaction, the products collected by centrifuge were washed by ethanol several times and dried at 80°C in air.

2.2. Characterization

The X-ray powder diffraction (XRD) pattern was recorded using a Japan Rigaku DMAX 2000 diffractometer equipped with graphite monochromatized Cu Kα radiation (λ=1.5418 Å) (40 Kv, 30 mA) irradiated at a scanning rate of 4 deg/min over a 2θ range from 10° to 80°. The field-emission scanning electron microscopy (FESEM) images were obtained using a JEOL JSM-7500F microscope operated at an acceleration voltage of 15 kV. A JEOL JEM-200CX microscope operating at 160 kV in the bright-field mode was used for transmission electron microscopy (TEM). Selected area electron diffraction (SAED) pattern was performed on a JEOL JEM-2010 electron microscope operating at 200kV and the binding energy of Mn was analyzed by a VG Scientific ESCLAB 220iXL X-ray photoelectron spectrometer (XPS). FT-IR spectra were collected using a Nicolet Avatar 370. The photo-excitation (PLE) and photo-luminescence (PL) spectra were measured using a HITACHI F-4600 FL Spectrophotometer and performed at room temperature and the luminescence decay in visible was recorded by using a FLS920 fluorescence spectrophotometer.

3. Results and discussion

3.1. XRD analysis of K_2SiF_6:Mn^{4+} nano/micro-particles

In the synthesized process of K_2SiF_6:Mn^{4+}, KOH/oleic acid quality radio and SiO_2 spheres/$KMnO_4$ molar ratio influence the microstructures and crystallinity of K_2SiF_6, Figure 1 shows the XRD patterns of some typical K_2SiF_6:Mn^{4+} samples, such as nanorods (Figure 1a and Figure 1b), micro-particles (Figure 1c). Their XRD patterns are indexed to the JCPDS card (07–0217) and no other impurity peaks are detected. These XRD results indicate that K_2SiF_6:Mn^{4+} can be successfully prepared by using an efficient one-step method in room ambient.

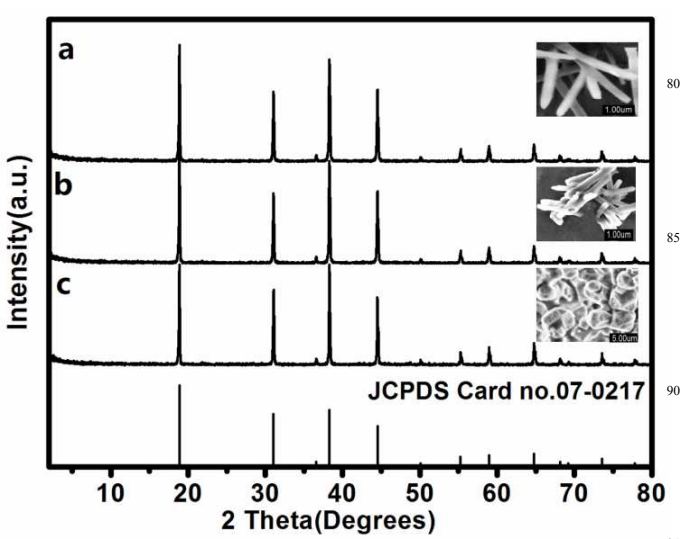

Figure 1. XRD patterns of typical K_2SiF_6:Mn^{4+} samples with different shapes.

3.2. The influencing factors in the shape controlled synthesis of K_2SiF_6:Mn^{4+}

In order to get a full understanding about the shape control of K_2SiF_6:Mn^{4+} in a reaction system, several important synthetic factors are investigated, including KOH/oleic acid quality ratio, different kinds of surfactants, SiO_2 spheres/$KMnO_4$ molar ratio , reaction time and so on. In the following paragraphs, the influence of these factors on the shape and microstructure of the products are commented in detail.

3.2.1. The influence of KOH/Oleic acid quality ratio in the mixed solvents.

Due to the different experimental methods, the different solubility of inorganic raw materials and the different reaction time, the morphologies of K_2SiF_6:Mn^{4+} are different from tradition morphologies in previous experimentals[2, 10, 11]. In our case, KOH/oleic acid quality ratio in mixed solvents plays an important role in the microstructure and growth. The morphology of K_2SiF_6:Mn^{4+} samples is regular changed by increasing KOH/oleic acid. Hence, we study the influence of the KOH/oleic acid quality ratio on the morphology of K_2SiF_6:Mn^{4+} samples at first. SiO_2 spheres/$KMnO_4$ molar ratio and reaction time are kept constant at 1:10, 30 min, respectively, KOH/oleic acid quality ratio is changed from 0.5:1, 1.2:1 to 2.5:1, and the total mixed solvent volume is 50 mL. The morphology and microstructure details of as prepared K_2SiF_6:Mn^{4+} samples are investigated by FESEM and TEM techniques. As shown in the Figure $2a_1$, when KOH/oleic acid quality ratio is 0.5:1, in other words, potassium oleate is to be less, it shows that the as-obtained products are composed of particles with the average size in the range of 1~2 μm. Careful observation from Figure $2a_2$ indicates that many particles appear uniform hexagonal facet, According to the image, the diameters are about 950 nm. By increasing the quality ratio of KOH/oleic acid, which is 1.2:1, as shown in Figure $2b_1$, the products grow into nanorods on a large scale. As shown in Figure $2b_2$, the individual nanorod structure has a length in the range of 1~2 μm and a width in the range of 300~700 nm. When KOH/oleic acid quality ratio is 2.5:1, at so high KOH quality, the products still maintain nanorods structures, but it is worth noting that their exact structures are obviously changed. The each nanorod has a length in the range of 4~6 μm through observating from Figure $2c_1$, however, very careful observation indicates that they are actually with a length of about 10 μm and a width of about 100 nm from Figure $2c_2$. From three insects in Figure 2, the corresponding fast Fourier transform (FFT) pattern is observed, show crystallographic planes (220) planes(Figure $2a_2$), (111) planes (Figure $2b_2$), (111) planes(Figure $2c_2$) of the K_2SiF_6, respectively. Therefore, nano-structure has similar growth planes. From above three samples, it is easy to find the tendency that increasing the amount of potassium oleate promotes the products growing into different shapes. To further investigate the influence of potassium oleate over the shape control, another series of contrast experiments were carried out. Some reports proved that oleic acid played a key part[12-15], but in our case, if there are no KOH are added into the mix solution, the products grow into micro-particles with a diameter of 5 μm. At the same time, we

also try to only increase or decrease the quality of oleic acid, but it does not work, the products still grow into particles, which indicates that oleic acid plays a secondary role. However, when KOH/oleic acid mole ratio is 1:1, which means that they react completely, the products grow into nanorods with a length of about 5 μm and a width of about 400 nm. In another contrast experiment, the quality of KOH is excessive, at the first time, we think the products grow longer nanorods by adding KOH, to our surprised, the morphology of K_2SiF_6:Mn^{4+} is particles with a diameter of 1 μm, which indicates that the influence of potassium oleate over the shape control is obvious and significant.

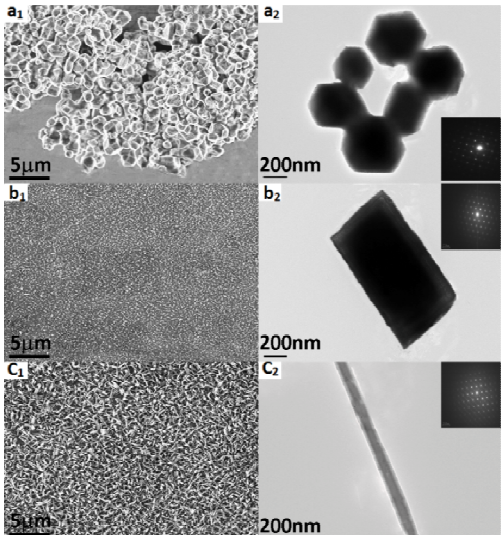

Figure 2. SEM and TEM images of K_2SiF_6:Mn^{4+} samples obtained at different KOH/oleic acid quality ratio: (a_1–a_2) 0.5:1, (b_1–b_2) 1.2:1 and (c_1–c_2) 2.5:1. SiO_2 spheres/$KMnO_4$ molar ratio and reaction time are kept constant at 1:10, 30 min, respectively.

In order to control the morphology of samples, many works tried to add some surface active agents in previous reports[16-18]. In our experimental range, it is necessary to understand the influencing factors in the formation of the nano structure by adding some surface active agents, such as PVP, cetyl trimethyl ammonium bromide, PEG-600 and sodium stearate and so on. The products turns out to be grown into some uniform particles with a diameter of 1 μm, no nanorods can be observed in the samples, which are obtained in the reactions using KOH and oleic acid. The result is shown in Figure $3a_1$ by using PVP in our solution. It is found that the products are fairly uniform particles, Figure $3a_2$ and Figure $3a_3$ is the TEM of the K_2SiF_6:Mn^{4+} and the selected area electron diffraction patterns of K_2SiF_6:Mn^{4+}, which reveals that the diameters of particles are about 980 nm. The corresponding fast Fourier transform (FFT) pattern shows crystallographic planes from Figure $3a_3$, in which the d spacing of 1.819 nm, 2.877 nm, 1.866 nm corresponds to (420) planes, (220) planes, (331) planes of the K_2SiF_6, respectively. Hence, we believe that $CH_3(CH_2)_7CH{=}CH(CH_2)_7COO^-$ ions should be responsible for the nano structure of K_2SiF_6:Mn^{4+}.

The FT-IR spectrum is used to prove the adsorption of $CH_3(CH_2)_7CH{=}CH(CH_2)_7COO^-$ ions. The FT-IR spectra of K_2SiF_6:Mn^{4+} obtained through using PVP and KOH/oleic acid/ethanol/deionized water are shown in Figure 3b.The IR bands at about 580 cm^{-1} are attributed to the $(-CH_2-)_n(n>4)$ bending vibration(ρ). Meanwhile, there is (C-H) and (-OH) at about 1025 cm^{-1} and 3455 cm^{-1}, respectively, but (-OH) is the OH wide band of the carboxyl. The IR bands at about 1388 cm^{-1} and 1531 cm^{-1} are attributed to the $(-CH_3)$ asymmetrical stretching vibration (νas), a common unit that is present in oleic acid. There is the C=O asymmetric stretching vibration (νas) at about 1663 cm^{-1}, the C=O asymmetric stretching vibration of $CH_3(CH_2)_7CH{=}CH(CH_2)_7COO^-$ ions is at a higher wavenumber, implying the presence of (–COOH)[19, 20].

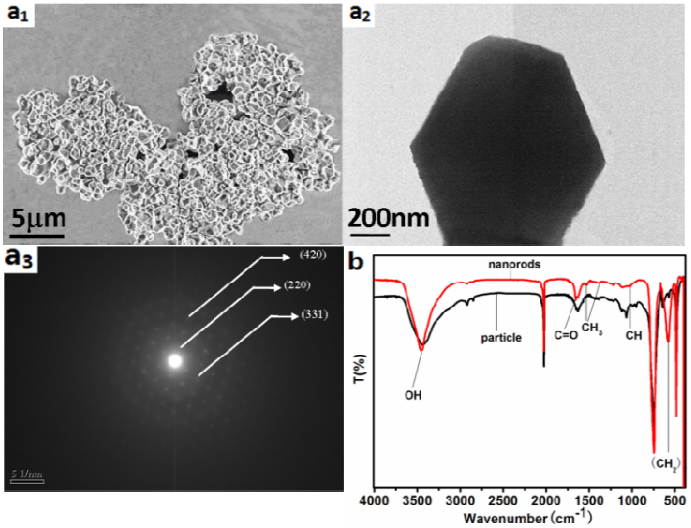

Figure 3. (a_1): SEM images of the K_2SiF_6:Mn^{4+} samples using PVP. (a_2): TEM images of K_2SiF_6:Mn^{4+}. (a_3): Selected area electron diffraction patterns of K_2SiF_6:Mn^{4+}. (b): The FT-IR spectra of K_2SiF_6:Mn^{4+} obtained through using PVP (black) and KOH/oleic acid/ethanol/deionized water (red), respectively.

3.2.2. The influence of SiO_2 spheres/$KMnO_4$ molar ratio.

In the above discussions about the influence of the KOH/oleic acid quality ratio, the samples are only prepared at the SiO_2 spheres/$KMnO_4$ molar ratio of 1:10. In our experiment, besides oleic acid provides K^+ ions, $KMnO_4$ also provides K^+ ions. The concentration of $KMnO_4$ changes in reaction holds a leading position. In order to further investigate the shape dependence on the amount of $KMnO_4$, SiO_2 spheres/$KMnO_4$ molar ratio changes from1:0.5, 1:15 to 1:50, three series of raw materials ratio dependent experiments are conducted in the 50 mL mixed solutions with KOH/oleic acid quality ratio of 2.5:1, reaction time is kept constant at 30 min. As shown in Figure $4a_1$, when the SiO_2 spheres/$KMnO_4$ molar ratio is 1:0.5, the products show nanorods morphologies on a large scale, these nanorods are uniform in dimension. Their length is almost about 200 nm and width is uniformly about 70 nm (Figure $4a_2$). When the SiO_2 spheres/$KMnO_4$ molar ratio is 1:15, the products grow into nanorods with a length of about 2~4 μm and a width of about 80~100 nm (Figure $4b_1$), which compared with the shown in Figure $3c_1$, it is found that the length of the products is becoming shorter. In the high resolution SEM picture from Figure $4b_2$, these nanorods are fairly even–distributed. As can be seen from Figure $4c_1$and Figure $4c_2$, when the SiO_2 spheres/$KMnO_4$ molar ratio is 1:50, the products consist of uniform particles, which have diameters of 1~2 μm.

Their SEM images reveal that the morphologies of $K_2SiF_6:Mn^{4+}$ change from nanorods to particles, with increasing $KMnO_4$ content in the mixed solution. We also try to synthesise the $K_2SiF_6:Mn^{4+}$samples in lower $KMnO_4$ content or in higher $KMnO_4$ content, but it is found that the products grow into shorter nanorods with lower $KMnO_4$ and larger particles with higher $KMnO_4$. Hence, from the above descriptions, when $KMnO_4$ concentration is low, in the other words, one of raw materials is not sufficient, so the achieved products that are shorter nanorods. By increasing $KMnO_4$ molar ratio, the concentration of $CH_3(CH_2)_7CH{=}CH(CH_2)_7COO^-$ is in a good range, and the particles grow along on direction continuously, therefore the longer nano rods are obtained, as shown in figure 4b. But, if the concentration of KMnO4 is too high, the reaction rate is so fast that the absorbed $CH_3(CH_2)_7CH{=}CH(CH_2)_7COO^-$ cannot control the morphology growth, so irregular micro particles are obtained, as show figure4c. Therefore, all these morphologies information indicate an appropriate $KMnO_4$ content makes the K_2SiF_6 crystal growth tend to be complete and perfect. We can find some evidence to support this point, Solvothermal synthesis of $NaYF_4$ nanocrystals[21], self-assembled cubic-phase and orthorhombic-phase BaF_2 nanocrystals are synthesized by LSS[22], time-dependent growth of CeF_3 nanoparticles[12] and the synthesis of highly uniform and monodisperse Ba_2ClF_3 microrods[15].

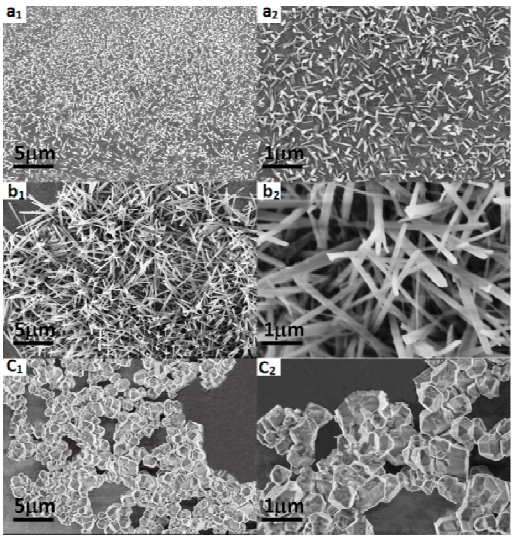

Figure 4. SEM images of $K_2SiF_6:Mn^{4+}$ samples obtained at different SiO_2 spheres/$KMnO_4$ molar ratio: (a_1–a_2) 1:0.5, (b_1–b_2) 1:15 and (c_1–c_2) 1:50. The quality ratio of KOH and oleic acid and reaction time are kept constant at 2.5:1, 30 min, respectively.

3.2.3. Effects of the reaction time

In order to more in-depth understanding of the evolution mechanism of the $K_2SiF_6:Mn^{4+}$ nanorods, the products obtained at different reaction time are observed by SEM shown in Figure 5. The quality ratio of KOH and oleic acid and SiO_2 spheres/$KMnO_4$ molar ratio are set as 2.5:1, 1:10, respectively. The time-dependent shape experiments indicate that the nanorods grow very slowly. As shown in the Figure 5a, reaction time is set as 10 min, the length of nanorods is almost about 80 nm and the width is uniformly about 50 nm. When the reaction time was added up to 20 min (Figure 5b), the obtained products consist of nanorods with a length of 400 nm and a width of 70 nm. When the reaction time is prolonged to 1 h, as shown in Figure 5c, a series of nanorods with a length of about 2~6 μm and a width of about 90 nm form the sample, which look more perfect and the size uniformity is greatly improved. Eventually, after 2 h, their morphologies are shown in Figure 5d. It is found that the length of nanorods is almost about 4~8 μm and the width is about 150 nm.

Based on the above time dependent experiments, the length is getting longer and these results indicate that reaction time have obvious effects on the nanorods, which indicate that morphologies of samples is manageable. Of course, other parameters, including temperature, the initial pH value and so on, also influence the morphologies of products, but we have no more opportunities to make any changes, because if the concentration of $KMnO_4$ is increased or KOH/ oleic acid ratio is higher, it will cause the size of $K_2SiF_6:Mn^{4+}$ greatly changes. Considering the above points, we do not introduce and discuss these factors here in detail.

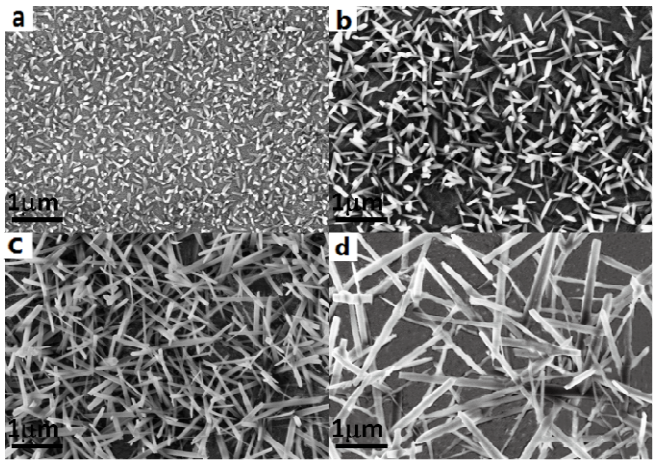

Figure 5. SEM images of $K_2SiF_6:Mn^{4+}$ samples obtained at different times: (a) 10 min (b) 20 min (c) 1 h (d) 2 h. The quality ratio of KOH and oleic acid and SiO_2 spheres/$KMnO_4$ molar ratio are set as 2.5:1, 1:10, respectively.

3.2.4. Growth mechanism for the nanorods.

A possible schematic illustration of formation mechanism of this nanorods structure is described as follows. Meanwhile, all the results indicate that the formation mechanism of the nanorods is so complicated that there is no single factor that can decide the morphology and size of the as-prepared nanocrystals. At first, oleic acid and KOH synthesize the potassium oleate, which has hydrophilic group and oleophilic group. Then prism seeds of $K_2SiF_6:Mn^{4+}$ quickly nucleate and grow, undergoing the self-assemble and dissolution-reconstruction process. When the quality ratio of KOH and oleic acid is about 0.5:1 or less or SiO_2 spheres/$KMnO_4$ molar ratio is about 1:50 or more, the adsorption of oleic acid molecules on the surface of $K_2SiF_6:Mn^{4+}$ is selective, which causes the limitation of some crystal orientation and reduces the rate of reaction. In the end, the particles are formed. However, when KOH/oleic acid quality ratio is about 2.5:1 or SiO_2 spheres/$KMnO_4$ molar ratio is about 1:10 or more than 1:50, the reaction process is possible as follows. After the addition of aqueous solution, an ion exchange process occurred

between oleic acid and K^+ to form potassium oleate under agitation, and simultaneously a phase transfer process occurred in which the K^+ ions shift from the aqueous solution to the solid phase of RCOOK[15]. Along with the addition of F^- and Si^{4+} in turn, the oleic acid capped K^+ reacted with $F^-$and Si^{4+} to form K_2SiF_6 nanorods precipitation under agitation. In short, the proportion of raw material controls the morphology of K_2SiF_6:Mn^{4+}. Meanwhile, the results may help in the control and manipulation of the shape and phase of various nanocrystals[23].

3.3. Luminescent properties of K_2SiF_6:Mn^{4+}

Figure 6 shows PLE and PL spectra of the K_2SiF_6:Mn^{4+} phosphor with different shapes. Mn^{4+} ion has the effective ion radius of r=0.54 Å and can be substituted for the Si^{4+} ion (r=0.40 Å) in the SiF_6^{2-} octahedra, but Mn^{2+}(r=0.83 Å) or Mn^{3+} ion (r=0.65 Å) does not perceptibly do so[24]. The peak at 365 nm originated from the transition$^4A_{2g}\rightarrow{}^4T_{1g}$ of the MnF_6^{2-}ion in K_2SiF_6, and the same energy separation as that for the$^4A_{2g}\rightarrow{}^4T_{2g}$ transition at ~460 nm. Meanwhile, the emission spectra excited at 365 nm and 460 nm are measured, respectively, which show similar shape, indicating that Mn^{4+} locates only one type of crystal site in K_2SiF_6. The relative intensity of emission spectrum excited at 460 nm is the strongest, which indicates it is ideal as a red phosphor for LEDs. The emissions centered at 615 nm, 632 nm and 649 nm, the peak at 632 nm and 649 nm are ascribed to $^2E\rightarrow{}^4A$ transition of the $3d^3$ electrons in the MnF_6^{2-}[25]. When these samples are irradiated by 365 nm UV emission lamp, it exhibits good red emission. Meanwhile, the relative intensity of emission spectrum is increased by the increasing KOH/oleic acid quality ratio. When KOH/oleic acid quality ratio is 2.5:1, nanorods have better luminescence properties than particles which are achieved. Therefore, nanorods own superior property.

To further investigate that nanorods have better luminescence properties, the XPS measurements are performed to examine powders. Chemical species of potassium, silicon, and fluorine, together with manganese species, have been detected on the powders. Figure 7 shows the XPS spectrum for Mn with different shapes, obtained at different KOH/oleic acid quality ratio 0.5:1, 1.2:1 and 2.5:1, but SiO_2 spheres/$KMnO_4$ molar ratio is 1:10, reaction time is kept constant at 30 min. The results indicate that Mn concentration in the red phosphor to be about 0.05 mol %, 0.3 mol % and 0.9 mol %, respectively. The XPS survey spectra in high magnification are shown in the supporting information. KOH/oleic acid quality ratio affects the absorption of Mn^{4+} ions is easy to be observed. In the mixed solution, $KMnO_4$ not only offers K^+ ions, but also offers Mn^{4+} ion. With increasing the amount of potassium oleate, Mn^{4+} ions are better absorbed and luminescence properties are improved. Thus, KOH/oleic acid is an important role to control the morphology and enhance luminescence properties of K_2SiF_6:Mn^{4+} phosphor. All results prove that nanorods have better luminescence properties than particles.

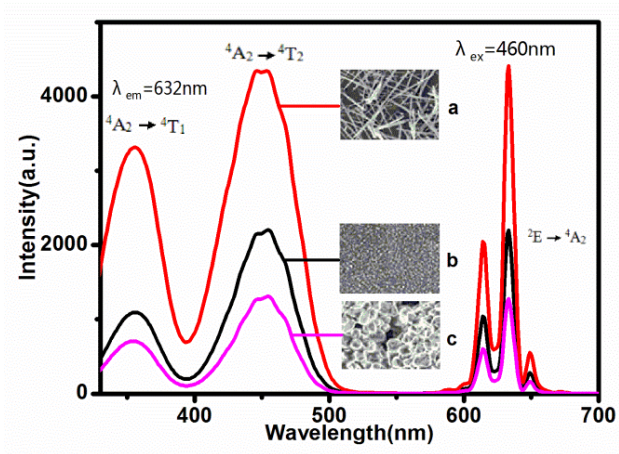

Figure 6. Luminescent properties of K_2SiF_6:Mn^{4+} with different shapes (λ_{em}=632 nm, λ_{ex}=460 nm) at various KOH/oleic acid quality ratios (a) 2.5: 1 (b) 1.2:1 and (c) 0.5:1. SiO_2 spheres/$KMnO_4$ molar ratio and reaction time are kept constant at 1:10, 30 min, respectively.

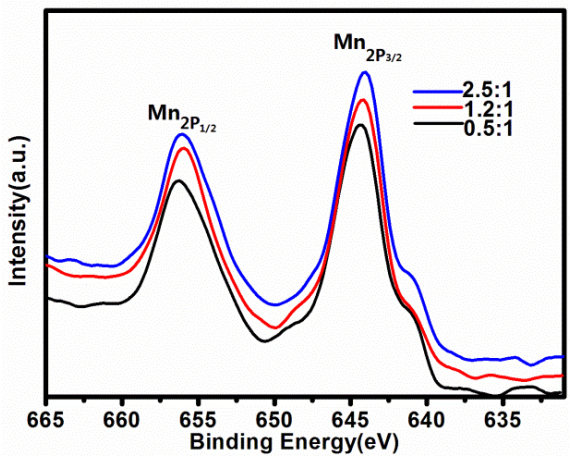

Figure 7. XPS spectra of Mn obtained in different shapes at various KOH/oleic acid quality ratios. SiO_2 spheres/$KMnO_4$ molar ratio and reaction time are kept constant at 1:10, 30 min, respectively.

Simultaneously, the pink powder phosphor that is different from the yellow powder phosphor achieved by other methods emits strong red luminescence under a UV lamp as shown in Figure 8 insets. Figure 8 indicates that SiO_2 spheres/$KMnO_4$ molar ratio is reduced, the relative intensity of emission spectrum is not increased. When the molar ratio is 1:10, the relative intensity is strongest. However, the molar ratio is less than 1:10, luminescence properties is weakening, which implies that not only SiO_2 spheres/$KMnO_4$ molar ratio is other factor, affects the morphology of K_2SiF_6:Mn^{4+}, but also the property.

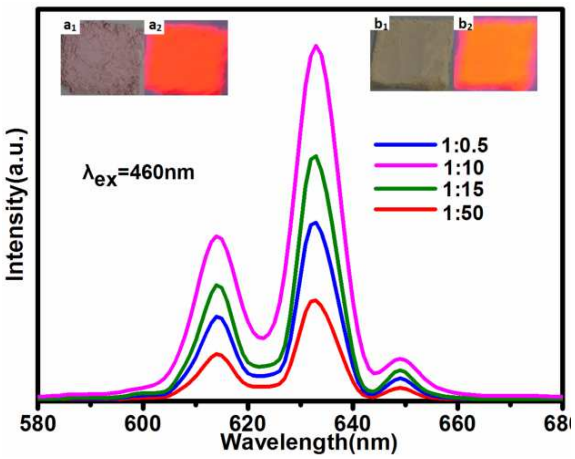

Figure 8. Emission spectra of red phosphor $K_2SiF_6:Mn^{4+}$ obtained at different SiO_2 spheres/$KMnO_4$ molar ratio. KOH/oleic acid quality ratio and reaction time are kept constant at 2.5:1, 30 min, respectively. Insets: digital photos of the phosphor $K_2SiF_6:Mn^{4+}$ nanorods(a_1, a_2) and particles (b_1, b_2) under (a_1, b_1) visible light and (a_2, b_2) 365 nm UV light excitation.

At the same time, the luminescence of this red phosphor is enhanced by increasing of reaction time up to 2 h (Figure 9), the increase of emission intensity after 30min reaction is presumably due to kinetics equilibrium of reaction and completing of crystallization, but emission intensity of 1h reaction and 2h reaction is similar, so there is no need to increase the reaction time and KOH/oleic acid quality ratio or SiO_2 spheres/$KMnO_4$ molar ratio needs to be well controlled. Otherwise, thermostability and lifetime of the samples are tested. The results suggest that $K_2SiF_6:Mn^{4+}$ nanorods have the same thermostability as $K_2SiF_6:Mn^{4+}$ particles, and the PL lifetimes τ determined are 8.17 ms for $K_2SiF_6:Mn^{4+}$ nanorods with a length of about 10 μm and a width of about 100 nm, 7.44 ms for $K_2SiF_6:Mn^{4+}$ nanorods with a length of 1~2 μm and a width of 300~700 nm, 5.39 ms for $K_2SiF_6:Mn^{4+}$ particles with 1 μm and 7.36 ms for $K_2SiF_6:Mn^{4+}$ particles with 10 μm. No large differences in τ can be observed between these various morphologies phosphors.

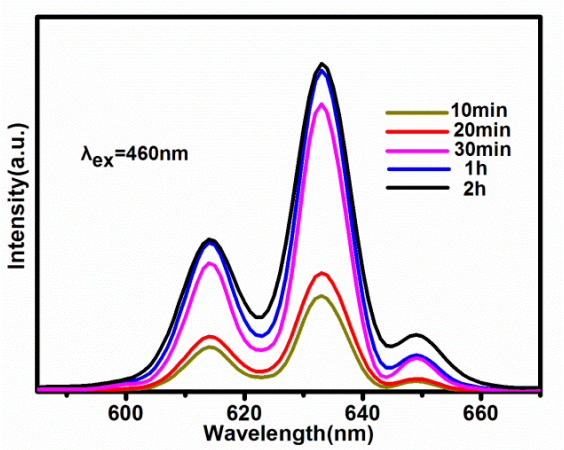

Figure 9. Emission spectra of red phosphor $K_2SiF_6:Mn^{4+}$ obtained from the various reaction times. KOH/oleic acid quality ratio and SiO_2 spheres/$KMnO_4$ molar ratio are set as 2.5:1, 1:10, respectively.

Conclusions

In conclusion, $K_2SiF_6:Mn^{4+}$ nanorods are synthesized by the dissolution–reconstruction–growth mechanism. In this precipitation process, the existence of potassium oleate is a key factor in the formation of nanorods structures. With increasing the quality ratio of KOH/oleic acid, the morphologies of $K_2SiF_6:Mn^{4+}$ are from particles to nanorods, which the diameter is from 1~2 μm to 300 nm~700 nm. SiO_2 spheres/$KMnO_4$ molar ratio is another key factor in the shape controlled synthesis. $K_2SiF_6:Mn^{4+}$ morphologies are from nanorods to particles, which the length is from 200 nm to 4 μm, with adding the molar ratio of SiO_2 spheres/$KMnO_4$. However, low KOH/oleic acid quality ratio and high SiO_2 spheres/$KMnO_4$ molar ratio are easy to produce particles structures. Under UV excitation, $K_2SiF_6:Mn^{4+}$ nanorods and particles samples show strong red emission, but nanorods samples show better luminescent properties and thermostability than particles.

Acknowledgements

This work is supported by Shanghai Science & Technology Committee (12521102501), Shanghai Educational Committee (11ZR1426500), Innovation Program of Shanghai Municipal Education Commission (14ZZ127), PCSIRT (IRT1269), and the Program of Shanghai Normal University (DZL124), Academic Leaders Training Program of Pudong Health Bureau of Shanghai (Grant No. PWRd2011-09)

Notes and references

# *Equal contribution as the first author*
[a] *The Education Ministry Key Lab of Resource Chemistry and Shanghai Key Laboratory of Rare Earth Functional Materials, Department of Chemistry, Shanghai Normal University, Shanghai 200234, People's Republic of China.*
[b] *Physics and Chemistry Test Lab, Shanghai Pudong New Area Center for Disease Control & Preverntion, Shanghai 200136, People's Republic of China.*
E-mail: liujie@shnu.edu.cn, xibinyu@shnu.edu.cn, mzhan@pdcdc.sh.cn

1. M. H. Du, *Journal of Materials Chemistry C*, 2014, **2**, 2475-2481.
2. S. Adachi and T. Takahashi, *Electrochemical and Solid-State Letters*, 2009, **12**, J20-J23.
3. Y. Arai, T. Takahashi and S. Adachi, *Optical Materials*, 2010, **32**, 1095-1101.
4. T.-D. Nguyen, C.-T. Dinh and T.-O. Do, *ACS Nano*, 2010, **4**, 2263-2273.
5. X. Jiang, Y. Pan, S. Huang, X. a. Chen, J. Wang and G. Liu, *Journal of Materials Chemistry C*, 2014, **2**, 2301-2306.
6. X. He and B. Yan, *Journal of Materials Chemistry C*, 2014, **2**, 2368-2374.
7. S. A. Khan, A. Günther, M. A. Schmidt and K. F. Jensen, *Langmuir*, 2004, **20**, 8604-8611.
8. R. Vacassy, R. J. Flatt, H. Hofmann, K. S. Choi and R. K. Singh, *Journal of Colloid and Interface Science*, 2000, **227**, 302-315.
9. X.-D. Wang, Z.-X. Shen, T. Sang, X.-B. Cheng, M.-F. Li, L.-Y. Chen and Z.-S. Wang, *Journal of Colloid and Interface Science*, 2010, **341**, 23-29.
10. C. Liao, R. Cao, Z. Ma, Y. Li, G. Dong, K. N. Sharafudeen and J. Qiu, *Journal of the American Ceramic Society*, 2013, **96**, 3552-3556.
11. T. Takahashi and S. Adachi, *Electrochemical and Solid-State Letters*, 2009, **12**, J69-J71.
12. S. Li, T. Xie, Q. Peng and Y. Li, *Chemistry – A European Journal*, 2009, **15**, 2512-2517.
13. G. Wang, Q. Peng and Y. Li, *Journal of the American Chemical Society*, 2009, **131**, 14200-14201.

14. G. Wang, Q. Peng and Y. Li, *Accounts of Chemical Research*, 2011, **44**, 322-332.
15. X. Zhang, C. Li, C. Zhang, J. Yang, Z. Quan, P. Yang and J. Lin, *Crystal Growth & Design*, 2008, **8**, 4564-4570.
16. H. Lee, S. E. Habas, S. Kweskin, D. Butcher, G. A. Somorjai and P. Yang, *Angewandte Chemie*, 2006, **118**, 7988-7992.
17. A. Wang, H. Yin, D. Liu, H. Wu, Y. Wada, M. Ren, Y. Xu, T. Jiang and X. Cheng, *Applied Surface Science*, 2007, **253**, 3311-3316.
18. Y. Yu, F.-P. Du, J. C. Yu, Y.-Y. Zhuang and P.-K. Wong, *Journal of Solid State Chemistry*, 2004, **177**, 4640-4647.
19. Y. Takeuchi, H. Yasukawa, Y. Yamaoka, N. Takahashi, C. Tamura, Y. Morimoto, S. Fukushima and R. C. Vasavada, *Chemical & pharmaceutical bulletin*, 1993, **41**, 1434-1437.
20. Y. Wang, J. F. Wong, X. Teng, X. Z. Lin and H. Yang, *Nano Letters*, 2003, **3**, 1555-1559.
21. L. Wang and Y. Li, *Chemistry of Materials*, 2007, **19**, 727-734.
22. T. Xie, S. Li, Q. Peng and Y. Li, *Angewandte Chemie*, 2009, **121**, 202-206.
23. X. Wang, J. Zhuang, Q. Peng and Y. Li, *Nature*, 2005, **437**, 121-124.
24. S. Adachi and T. Takahashi, *Journal of Applied Physics*, 2008, **104**.
25. A. Takahiro and A. Sadao, *Japanese Journal of Applied Physics*, 2011, **50**, 092401.

Shape-controlled synthesis of $K_2SiF_6:Mn^{4+}$ nanorods phosphor and luminescent properties

Xiaoqing Li, Jie Liu*, Pujun Liu, Zhiling Yao, Jiajun Chen, Hui Yao, Xibin Yu*

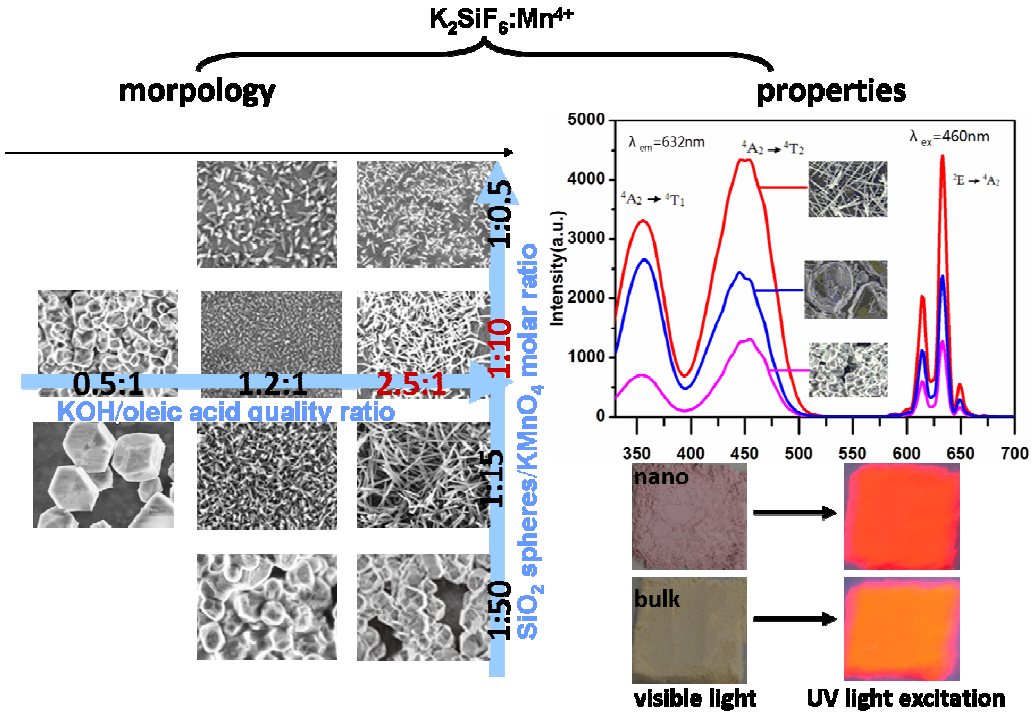

A red phosphor $K_2SiF_6:Mn^{4+}$ nanorod is successfully prepared through an efficient one-step method at room temperature in 30 min. Under UV excitation, $K_2SiF_6:Mn^{4+}$ nanorods show better red emission corresponding to the characteristic lines of Mn^{4+}, compared to bulk materials.